Diverse self-sustained oscillatory patterns and their mechanisms in excitable small-world networks

Yu Qian,[1,2,*] Xuhong Liao,[1] Xiaodong Huang,[1] Yuanyuan Mi,[1] Lisheng Zhang,[1] and Gang Hu[1,3,†]
[1]*Department of Physics, Beijing Normal University, Beijing 100875, China*
[2]*Nonlinear Research Institute, Baoji University of Arts and Sciences, Baoji 721007, China*
[3]*Beijing-Hong Kong-Singapore Joint Center of Nonlinear and Complex Systems, Beijing Normal University Branch, Beijing, China*
(Received 21 April 2010; revised manuscript received 26 July 2010; published 13 August 2010)

Diverse self-sustained oscillatory patterns and their mechanisms in small-world networks (SWNs) of excitable nodes are studied. Spatiotemporal patterns of SWNs are sensitive to long-range connection probability P and coupling intensity D. By varying P in wide range with fixed D, we observe totally six types of asymptotic states: pure spiral waves, pure self-sustained target waves, patterns of mixtured spirals and target waves, pseudospiral turbulence, synchronizing oscillations, and rest state. The parameter conditions for all these states are specified, and the mechanisms of these states are heuristically explained. In particular, the mechanism of emergence and annihilation of synchronizing oscillations is explained by using the shortest path length analysis.

DOI: 10.1103/PhysRevE.82.026107 PACS number(s): 82.40.Ck, 05.65.+b, 89.75.Hc

I. INTRODUCTION

A regular lattice with elements persisting excitable local dynamics is called an excitable medium [1,2]. Spatiotemporal pattern formation in excitable media has been attracted much attention during the last 30 years, not least because it is observed in a wide variety of natural systems, ranging from physical [3,4] to chemical systems such as Belousov-Zhabotinsky [5]. The interesting nonlinear dynamics of such patterns and their potential applications in various biological [6,7] or physiological [8] systems make them imperative to be understood. Spiral waves and target waves are two typical and important spatiotemporal patterns observed in these excitable systems [3,9]. Spiral waves can self-organize in the cardiac tissues and can self-sustain in autonomous systems with the spiral tips serving as the oscillation sources, while target waves can exist only by external pacings, such as the sinoatrial node performing as the pacing of the synchronous electrical waves in the intact heart, and can never exist in autonomous regular excitable media.

So far most of the research studying pattern dynamics of excitable tissues has focused on locally and regularly coupled media, and little has been known on the influences of long-range connections (LRCs) on the system dynamics. However, in many realistic systems of great importance the consideration of regular lattices may not yield adequate description given that distant elements may interact. Recently Watts and Strogatz proposed the so-called "small-world" network (SWN) model that takes into account both local and long-range interactions [10]. It was found that the existence of a small fraction of LRCs can essentially change the features of the given media and plays very important role in determining the system behaviors [11–16]. Further investigations showed that many realistic systems, in particular neural systems, indeed display the small-world properties, and these small-world structures and LRCs do play crucial roles in deciding the functions of systems. In the autonomous regular excitable media spiral waves are the unique self-sustained oscillating patterns. However, in excitable SWNs much richer self-organized oscillatory patterns have been revealed, such as self-sustained target waves and synchronizing oscillations [17–24]. The mechanisms underlying these new types of oscillations are however still not completely clear. In our recent work [25], we have proposed a method of *dominant phase-advanced driving* to reveal the oscillation sources of self-sustained target waves. The mechanism of synchronizing oscillation is still unknown. Moreover, the parameter conditions for different states of SWNs have not been systematically investigated. All of these are the tasks of the present paper.

In this paper we use a simple model, Bär-Eiswirth model, which has been widely used for discussing excitable dynamics, to study the diverse self-sustained oscillatory patterns of excitable SWNs by varying the LRC probability P in wide range with fixed coupling intensity D. Six types of asymptotic states have been observed: pure spiral waves, pure self-sustained target waves, patterns of mixtured spirals and target waves, pseudospiral turbulence, synchronizing oscillations, and rest state. The parameter conditions for these states are specified and the mechanisms of these states are heuristically explained. In particular, the mechanism of emergence and annihilation of synchronizing oscillations is explained by using the shortest path length (SPL) analysis.

II. MODEL AND DIFFERENT STATES IN EXCITABLE SWNs

We take a two-dimensional (2D) Bär-Eiswirth model [26] as our example:

$$\dot{u}_{i,j} = -\frac{1}{\epsilon}u_{i,j}(u_{i,j}-1)\left(u_{i,j}-\frac{v_{i,j}+b}{a}\right)+D_{i,j},$$

$$D_{i,j} = D(u_{i-1,j}+u_{i+1,j}+u_{i,j-1}+u_{i,j+1}-4u_{i,j}), \qquad (1a)$$

*qianyu0272@163.com
†ganghu@bnu.edu.cn

$$\dot{v}_{i,j} = f(u_{i,j}) - v_{i,j}, \tag{1b}$$

where $f(u_{i,j})=0$ for $u_{i,j}<\frac{1}{3}$, $f(u_{i,j})=1-6.75u_{i,j}(u_{i,j}-1)^2$ for $\frac{1}{3}\leq u_{i,j}\leq 1$, and $f(u_{i,j})=1$ for $u_{i,j}>1$. Here, u and v are the activator and the inhibitor variables, respectively; ϵ is the ratio of their temporal scales; and the dimensionless parameters a and b denote the activator kinetics with b effectively controlling the excitation threshold of the system. The system parameters are kept throughout this paper as $a=0.84$, $b=0.07$, and $\epsilon=0.04$. Therefore, the local cell can follow a typically excitable dynamics and the spiral patterns formed under these parameters are periodic [26]. D is the coupling intensity and it is selected as a controllable parameter. In the present paper we consider 100×100 cells in 2D regular lattices with constant and homogeneous nearest couplings. In addition to the diffusive coupling, we introduce LRCs such that each cell receives unidirectionally a connection from a randomly chosen cell with probability P [19]. These LRCs are chosen initially and kept for the durations of the system evolutions. We thus add an additional coupling term $D'_{i,j}$ to Eq. (1a) as

$$\dot{u}_{i,j} = -\frac{1}{\epsilon}u_{i,j}(u_{i,j}-1)\left(u_{i,j}-\frac{v_{i,j}+b}{a}\right)+D_{i,j}+D'_{i,j},$$

$$D'_{i,j}=\begin{cases} D(u_{i',j'}-u_{i,j}) & \text{if node } (i,j) \text{ receives} \\ & \text{an interaction from node } (i',j') \\ 0, & \text{otherwise,} \end{cases}$$

$$\dot{v}_{i,j} = f(u_{i,j}) - v_{i,j}. \tag{2}$$

Here, site (i',j') is randomly chosen in the 2D lattice. The equations are integrated by the second-order Runge-Kutta scheme with the time step $\Delta t=0.031$ and the no-flux boundary condition is used. For every simulation we use the random initial condition, i.e., the initial values of $u_{i,j}$ and $v_{i,j}$ of each sites are randomly given between 0 and 1. The spatiotemporal pattern formation in excitable SWNs is studied after getting rid of the starting 10 000 transient steps.

In simulations, we find that the LRC probability P and the coupling intensity D can strongly influence the spatiotemporal dynamics of the given system, and then we first study the system behaviors by widely varying these two parameters. For each pair of (P,D), we take 50 samples of SWNs with different random initial conditions and different random network structures, and measure the quantities of $u_{i,j}(t)$ and $v_{i,j}(t)$. Here, we define the averages of u variable as

$$\langle u(t)\rangle = (1/N^2)\Sigma_{i,j=1}^{N=100}u_{i,j}(t)$$

and v variable as

$$\langle v(t)\rangle = (1/N^2)\Sigma_{i,j=1}^{N=100}v_{i,j}(t),$$

and use the maximum value of $\langle u(t)\rangle[u_{max}=\max\{\langle u(t)\rangle\}]$ to classify the system state. Figure 1 shows three essentially distinct regions for different parameter combinations of P and D. The red region represents that in all the 50 samples the system totally develops from the random initial conditions into the rest state classified by $u_{max}=0$. In the purple domain we observe nonzero but small $u_{max}(u_{max}<0.5)$,

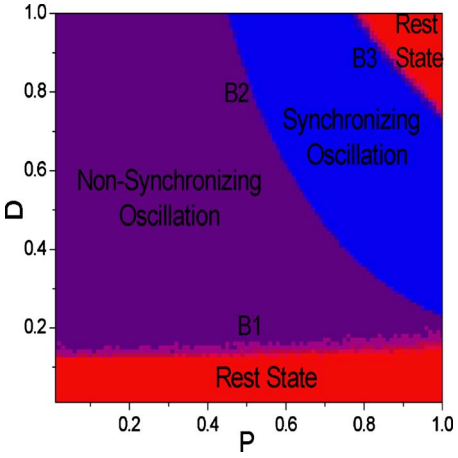

FIG. 1. (Color online) Three distinct regions for different parameter combinations of P and D. The red, purple, and blue regions represent that in all the 50 samples the system totally develops from the random initial conditions and arbitrary network structures into the rest state, the nonsynchronizing oscillation states, and the synchronizing oscillation states, respectively. Coexistence of two types of states are observed on the narrow strips between different colored domains (B1: nonsynchronizing oscillations and the rest state; B2: nonsynchronizing and synchronizing oscillations; B3: synchronizing oscillations and the rest state).

where the system states are dominated by various spiral and target wave patterns. In these patterns different cells have different phases and they are not synchronized in their motions, and then we call these states as nonsynchronizing oscillatory states. In the blue region u_{max} is very high (nearly equal to 1). This indicates that most of the cells are synchronously excited at u_{max}, and then we call these states as synchronizing oscillations. The transition colors between different state domains mean that in these parameter regions there are some probabilities with which the system evolve into different states of the nearby domains. For instance, at the transition between the blue (synchronizing oscillation) and red (rest state) parameter regions (see B3 in Figs. 1 and 2) the system evolves into synchronizing oscillatory states for a part of initial conditions and network structures while into the rest state for the other part of samples. In the following, we will keep the coupling intensity $D=1.0$ and vary the LRC probability P. We will focus our investigation on how LRCs influence the spatiotemporal pattern formation in the excitable SWNs.

Black squares in Figs. 2(a)–2(c) show the probabilities for the system $(N=100)$ to evolve into different spatiotemporal patterns with increasing P for fixed $D=1.0$. Generally speaking, the asymptotic spatiotemporal dynamics can be divided into three categories. First, for small P, the states of the system are characterized, after initial transient periods, by nonsynchronizing oscillations (various spiral and target wave patterns). Second, when P reaches a critical value ($P_c=0.45$ for $D=1.0$), synchronizing oscillations emerge and dominate the system after a short transient P region between $0.45\leq P\leq 0.46$, where both nonsynchronizing and synchronizing oscillations can be observed, depending on different initial conditions. In the blue synchronizing oscillation re-

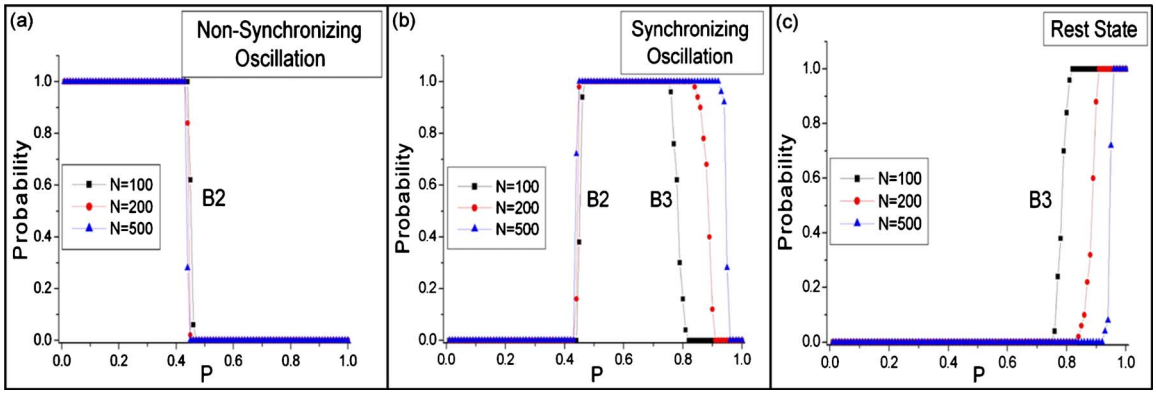

FIG. 2. (Color online) Probabilities for the system with three different sizes [$N=100$ (black square), $N=200$ (red circle), and $N=500$ (blue triangle)] evolving into (a) nonsynchronizing oscillations, (b) synchronizing oscillations, and (c) the rest state with increasing the LRC probability P for the fixed coupling intensity $D=1.0$. At various transition regions we can observe that different types of states coexist, i.e., coexistence between nonsynchronizing and synchronizing oscillations in (a) (B2), synchronizing oscillations and the rest state in (c) (B3), and both coexistences in (b) (B2 and B3).

gion a large fraction of cells get simultaneously active, and then refractory, in a periodic manner. Third, the self-sustained oscillatory activity begins to cease after $P \geq 0.76$ and the system totally falls into the rest state for $P \geq 0.82$. In the crossover domain $0.76 \leq P \leq 0.81$ we observe coexistence of synchronizing oscillations and the rest state for different initial conditions. A larger system size (red circles for $N=200$ and blue triangles for $N=500$) has been considered for the finite-size effects on the discontinuous transition. From these two sets of data, we can find that the critical values for the transition from nonsynchronizing oscillations to synchronizing oscillations are all around 0.45 and are independent of the system size N^2, while the system-size-dependent critical values are found when the system undergoes the transition from synchronizing oscillations to the rest state. For a larger system size, more LRCs are needed to reach the rest state.

To investigate these oscillatory states in detail, we plot the distributions of u_{max} and oscillation period T of the system versus the LRC probability P in the oscillatory region $0.01 \leq P \leq 0.81$ in Figs. 3(a) and 3(b), respectively. Figure 3(a) shows the statistical results of u_{max} with each of data computed for a given P by 100 samples. When P is small the system is in the nonsynchronizing oscillation region and u_{max} is low (i.e., $u_{max} < 0.5$), while u_{max} is high for the synchronizing oscillation with large P. In the transient region B2 both low and high values of u_{max} have been revealed simultaneously for the same P. In Fig. 3(b) we do the same as in Fig. 3(a) for T vs P. Besides the remarkable transition from nonsynchronizing region to synchronizing region as shown in Fig. 3(a), clearly two period bands have been found in the nonsynchronizing oscillation domain for small P ($P \leq 0.12$). It indicates that in this small connection probability region the system has two types of stable nonsynchronizing oscillations; one has a period larger than the other. Increasing P, these two period bands merge to a single band after $P \geq 0.13$. By further increasing P, the system undergoes discontinuous transitions: T jumps up from the lower band at $P=0.47$ and jumps down from the upper band at $P=0.44$, and the transient region B2 is between $0.45 \leq P \leq 0.46$. All these different T bands correspond to characteristically distinctive self-sustained oscillatory patterns, which will be analyzed in detail in the following sections.

III. FOUR SELF-SUSTAINED NONSYNCHRONIZING OSCILLATORY PATTERNS OF EXCITABLE SWNs

First we investigate the system dynamics in the two bands in Fig. 3(b) for small P ($P=0.01$). Two different kinds of spatiotemporal patterns have been found, pure single or multiple spiral waves and pure self-sustained target waves, which have been shown in Figs. 4(a) and 4(b), respectively. Figures 4(c) and 4(d) show the periodic time series of $\langle u(t) \rangle$ and $\langle v(t) \rangle$ of spiral waves [Fig. 4(a)] and self-sustained target waves [Fig. 4(b)], respectively. The maximum values of $\langle u(t) \rangle$ for spiral and target waves are about 0.331 and 0.293, and both are much lower than the value of synchronous state

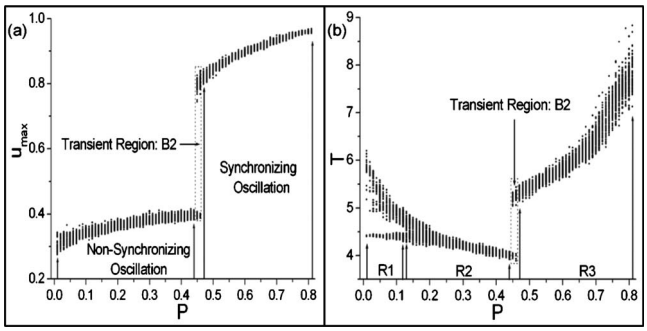

FIG. 3. (a) Distributions of u_{max} of the system versus the LRC probability P. When P is small the system is in the nonsynchronizing oscillation region and u_{max} is low, while u_{max} is high for the synchronizing oscillation with large P. In the transient region B2 both low and high values of u_{max} have been revealed simultaneously for the same P. (b) The same as (a) with oscillation period plotted vs P. Note that besides the discontinuous jump around the transient region B2, there are two branches of period distribution in the range of $0.01 < P \leq 0.12$ in the nonsynchronizing oscillations. The single period band jumps up (jumps down) around 0.47 (0.44).

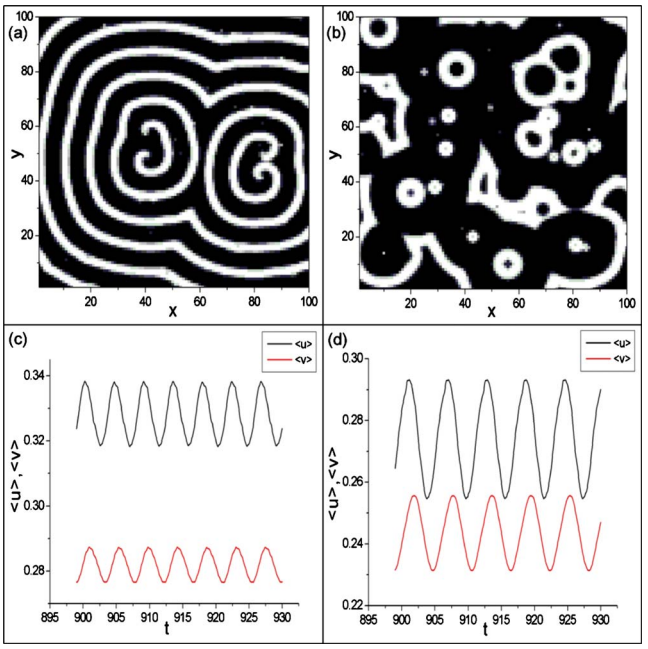

FIG. 4. (Color online) $P=0.01$. (a) and (b) Snapshots of the spatial profile of $u_{i,j}$ realized from random initial conditions. (a) Spiral waves realized from a certain set of initial conditions. (b) Self-sustained target waves realized from another set of initial conditions. (c) and (d) Time series $[\langle u(t)\rangle, \langle v(t)\rangle]$ of patterns (a) and (b), respectively.

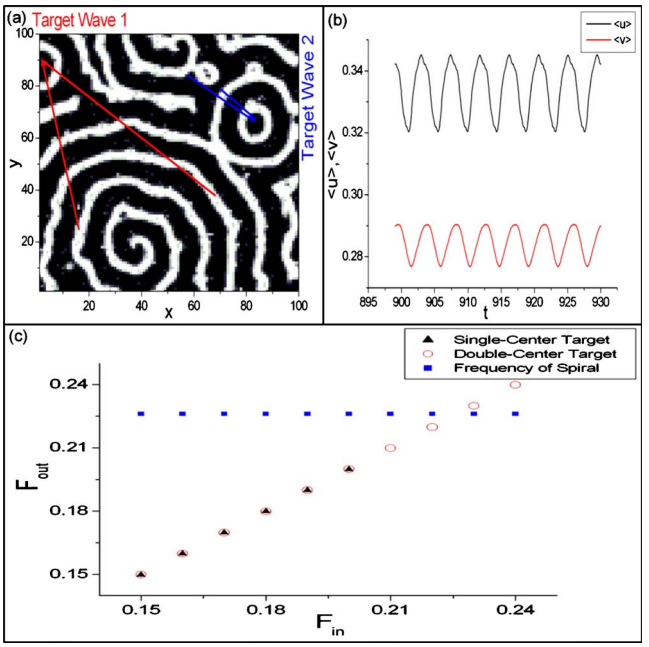

FIG. 5. (Color online) $P=0.15$. (a) Snapshot of the spatial profile of $u_{i,j}$ realized from random initial condition. (b) Time series $[\langle u(t)\rangle, \langle v(t)\rangle]$ of pattern (a). (c) 1:1 periodic response frequencies of target waves generated by a single pacing (black triangle: single-center target) and two pacings (red circle: double-center target). The blue squares show the frequency of spiral. It is found that the double-center target waves can reach larger maximum frequency than the single-center target.

($u_{max} \approx 1$) and we thus classify these two kinds of spatiotemporal patterns as nonsynchronizing oscillations. The oscillation sources of these two kinds of patterns are known clearly. For spiral waves [Fig. 4(a)], spiral tips serve as the sources to support the oscillation and the waves propagate from the spiral tips to boundary. For self-sustained target waves [Fig. 4(b)], successively phase-advanced driven loops have been revealed recently playing the role of oscillation sources [25]. In the present paper we go further to study in detail the influences of small-world structures to the dynamic characteristics of these spiral and target waves. In Fig. 1 we specify the parameter region for spiral and target waves, and we find that these two types of waves always coexist in the entire purple region. An interesting phenomenon is that in the region $P \leq 0.12$ [R1 in Fig. 3(b)] spiral and target waves coexist for the same parameter set, but they can never coexist in the same spatiotemporal pattern, i.e., the system is dominated by either spirals or targets. We thus call these patterns as pure spiral or pure target wave patterns. The reason is that in R1 region the frequency of spiral waves is always higher than that of the self-sustained target waves, and whenever both types of waves appear simultaneously in a same pattern due to certain initial conditions, the spiral waves must win the competition against the target waves and control the whole system. Therefore, target waves can asymptotically survive in a pattern only where no spiral remains, and spiral must kill all targets whenever they are produced simultaneously by certain initial conditions. This competition mechanism leads to states of the so-called "pure spiral" or "pure target" waves. In this bistable parameter region we also find that even for the same network structure, we can get spiral waves or self-sustained target waves for different random initial conditions. For a given initial condition all the spatial sites can be regarded to set into three different states: excited, refractory, and excitable states. The excited nodes can excite target waves as the target centers. If target wave fronts induced by these target centers encounter some sufficiently large refractory regions, the wave fronts can break there to produce wave tips, and then the system will evolve into spiral wave states. However, if these target wave fronts can all propagate smoothly and self-organize a successively phase-advanced driving loop, then they dominate the system with self-sustained target waves. From the above analysis, spiral waves have much larger probability of observation since from random initial conditions the probability to form sufficiently large refractory regions must be large. This is indeed the case in our simulations. For $P=0.01$, the probabilities of spirals and targets are 66% and 34%, respectively.

With increasing of P the period of pure target waves decreases. When $P \geq 0.13$, two period bands, one for spiral waves and the other for target waves, become merged. In the band region R2, besides the pure spiral waves as in Fig. 4(a) and pure self-sustained target waves as in Fig. 4(b), we observe patterns with both spiral and target waves mixtured (Fig. 5) and pseudospiral turbulence (Fig. 6). In Fig. 5(a) we take $P=0.15$ and show a typical example of mixtured patterns with both spiral and target waves. Figure 5(b) shows the corresponding $\langle u(t)\rangle$ and $\langle v(t)\rangle$ of Fig. 5(a). The maximum value of $\langle u(t)\rangle$ for this new spatiotemporal pattern is about 0.345 and thus the state is also in the domain of non-

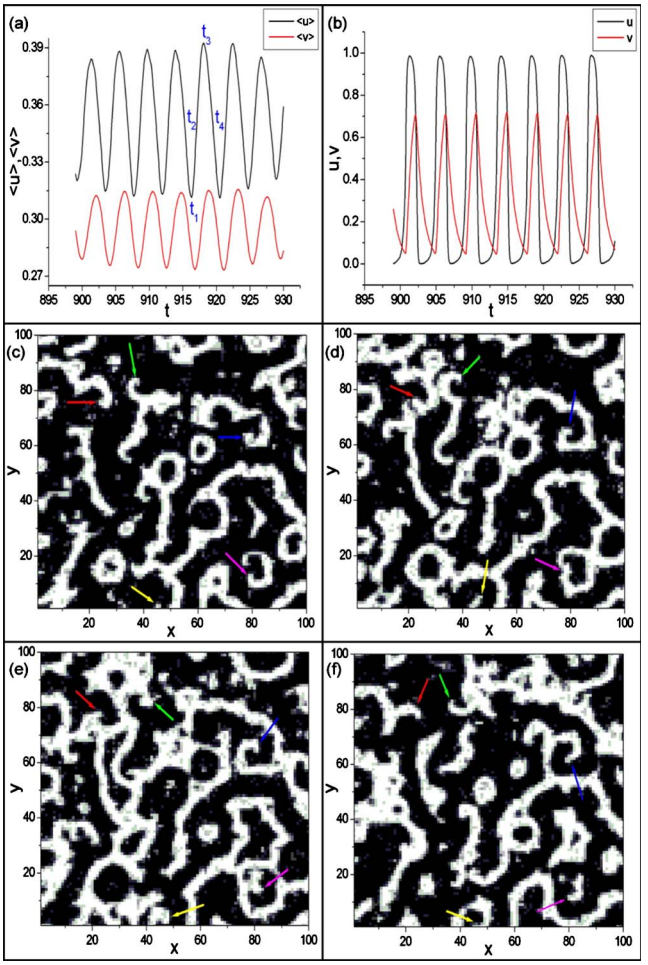

FIG. 6. (Color online) $P=0.30$. (a) Time series $[\langle u(t)\rangle,\langle v(t)\rangle]$ of a spiral turbulent pattern. Note that the periodicity of $[\langle u(t)\rangle,\langle v(t)\rangle]$ is lost, unlike Figs. 4 and 5. (b) Time series $[u(t),v(t)]$ of a spatial site (80,60) randomly chosen in the 2D apace. (c)–(f) Snapshots of the spatial profile of $u_{i,j}$ obtained at four moments indicated in (a). (c) $t=t_1$, (d) $t=t_2$, (e) $t=t_3$, and (f) $t=t_4$.

synchronizing oscillation region. However, the essential difference between Figs. 4 and 5 is that in the former spirals and targets exist separately in different patterns (from different initial conditions), while in the latter both spirals and targets appear simultaneously in the asymptotic state of a given pattern. The key reason for this difference is that in Fig. 5(a) all the target waves are generated by multiple (at least two) LRCs, and these targets are called multicenter targets. Further study show that 1:1 periodic response frequencies of target waves generated by pacing sources have certain maximum values, and these maximum frequencies can increase as they are generated by more pacing sources as shown in Fig. 5(c). In SWNs all LRCs play the role of pacing sources. For small P almost all target waves are generated by only single LRC. In this case [R1 region in Fig. 3(b)] the maximum frequency of possible target waves is low [see the black triangle for single-center target in Fig. 5(c)] and is lower than that of spiral frequency (see blue squares for spiral). Spiral waves can thus not generate new target waves by LRCs. On the contrary spiral waves can kill all existing target waves (if they exist in the transient period due to a certain initial condition) according to the competition law: high-frequency waves kill low-frequency waves. Therefore, we observe pure spirals or pure target waves in R1 region. The R2 region with larger P spiral has a larger probability to generate target waves via two or more LRCs. Since these target waves can have the same frequency as spiral waves (see the red circle for double-center target), they can survive and coexist with spirals in the same patterns. For instance, in Fig. 5(a) two centers of target wave 1 indicated by two red arrowed lines are all driven by the same spiral, and the two centers of target wave 2 indicated by two blue arrowed lines are driven one by a spiral wave and the other by the wave emitted from itself. These double-center target waves can reach larger maximum frequency which is the same as spiral than the single-center target. So they can coexist with spirals in the same pattern.

With more random LRCs, spatiotemporal patterns become chaotic. In Fig. 6 we fix $P=0.30$ and observe spiral turbulence in the nonsynchronizing oscillation region. Figures 6(a) and 6(b) show for a typical spiral turbulence pattern the time series of the average $\langle u(t)\rangle,\langle v(t)\rangle$ of the whole system and $u(t),v(t)$ of a single space node (80,60) randomly chosen in the 2D space, respectively. Figures 6(c)–6(f) show the snapshots of the given state at the four different moments indicated in Fig. 6(a). The moments t_1 and t_3 are at the instants of the maximum and minimum $\langle u(t)\rangle$ in a period while t_2 and t_4 are the moments corresponding to middle $\langle u(t)\rangle$ values. The snapshots at all these four moments look similar and there are no distinct differences between these patterns. This indicates that the spiral turbulence has temporal translational symmetry. This spiral turbulence is a kind of pseudoturbulence. For the real spiral turbulence spiral tips move randomly in the 2D space and they are generated and annihilated also randomly. Moreover, the time series of single sites are chaotic. In our case of pseudospiral turbulence, the dynamics of single site is nearly periodic as shown in Fig. 6(b). All spiral tips are located at fixed positions in the 2D space (see the arrowed sites in Fig. 6). The reason for these seemly random spatial patterns is that there are a large number of waves generated by LRCs, and these waves collide, and they collide also with the waves emitted from the fixed spiral tips. Therefore, the waves emitted from these fixed spiral tips are destroyed randomly by these random waves and cannot propagate to the whole media regularly, and these collision mechanisms produce the randomlike spatial patterns in Fig. 6.

IV. SELF-SUSTAINED SYNCHRONIZING OSCILLATIONS AND REST STATE

When the LRC probability P reaches a critical value (B2 in Figs. 1 and 2) we observe a discontinuous transition from nonsynchronizing oscillations to synchronizing ones. Typical time evolutions of averages $\langle u(t)\rangle$ and $\langle v(t)\rangle$ are shown in Fig. 7(a) with $P=0.75$. The maximum value of $\langle u(t)\rangle$ reaches nearly $u_{max}\approx 1.0$, and this indicates that the system exhibit synchronizing excitations at the moments of maximum $\langle u(t)\rangle$, i.e., a large fraction of the system is excited simultaneously, and then decays to refractory states synchronously.

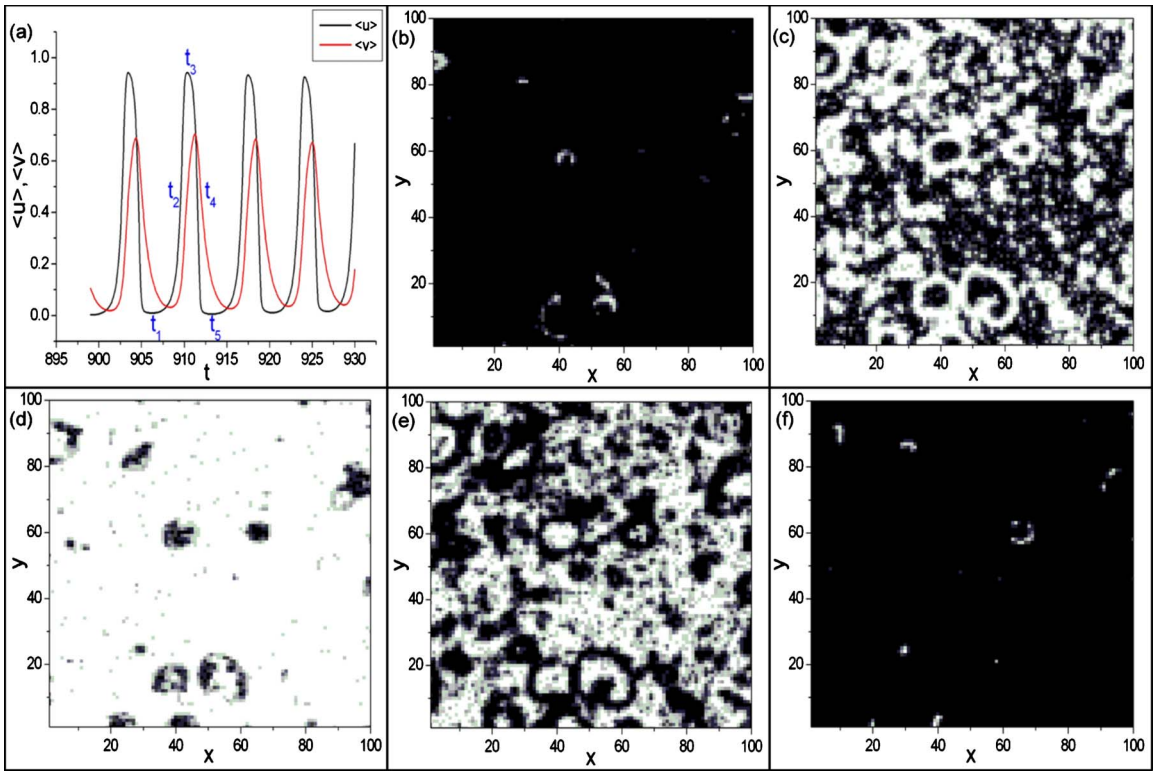

FIG. 7. (Color online) $P=0.75$. (a) Time series $[\langle u(t)\rangle, \langle v(t)\rangle]$ of the synchronizing oscillatory pattern. (b)–(f) Snapshots of the spatial profile of $u_{i,j}$ obtained at five moments indicated in (a). (b) $t=t_1$, (c) $t=t_2$, (d) $t=t_3$, (e) $t=t_4$, and (f) $t=t_5$.

Snapshots of the state at five instantaneous moments indicated in Fig. 7(a) are shown in Figs. 7(b)–7(f). These five spatiotemporal patterns are remarkably different from the spatiotemporal patterns shown in Fig. 6. In Fig. 6 all snapshots have no considerable difference, i.e., the spatiotemporal patterns of pseudospiral turbulence have approximately time translational symmetry of all cells. In sharp contrast to Fig. 6, Figs. 7(b) and 7(f) show patterns with most of the cells being at the rest states while Fig. 7(d) presents synchronous excitations of most of the cells. In these figures the system states are dramatically different for different time moments and the approximate time translational symmetry is lost completely. This is the reason for the discontinuous jumps in Fig. 3.

It should be emphasized that the synchronization shown in Fig. 7 can never be complete. In Figs. 7(b) and 7(f) we can still see that some cells do not step synchronously with most of the cells, and they are excited when most of other spatial sites are in the refractory state. This minority of cells are crucially important, called "antiphase wave tips." These antiphase wave tips can be formed by two processes: first, part of the target wave fronts induced by some LRCs encounter the refractory regions where wave fronts break to produce antiphase wave tips; second, some of the target wave fronts collide and yield new tips. These wave tips in very small fraction of cells play the role as the excitation sources to stimulate the system from the almost all "dead" states in Fig. 7(b) and then carry on the oscillatory activity of the whole system to the next cycle in Fig. 7(f). Because of the excitations by a large number of LRCs, and also because of local couplings around all the cells excited by the LRCs, most of spatial sites can be excited almost simultaneously by these few oscillation sources and the whole system exhibits the synchronizing oscillations which can be seen in Fig. 7(d) at the moment when $\langle u(t)\rangle$ approximates to 1.0. This mechanism differs essentially from that of Fig. 6 where some fixed oscillation sources (spiral tips) persistently emit waves and maintain oscillations of spiral turbulence.

For even larger P, the huge number of shortcuts can guarantee simultaneous spread of excitation to nearly all cells. As the result most of the spatial sites are in the refractory state also simultaneously, and thus not enough susceptible cells are left to sustain the excitation of the system. So for sufficiently large P the system falls into rest state after a short transient.

V. MECHANISM OF EMERGENCE AND ANNIHILATION OF SYNCHRONIZING OSCILLATION

To explore the mechanism underlying the transitions from nonsynchronizing oscillations to synchronizing ones and from synchronizing oscillations to the rest state (shown in Figs. 1 and 2 around the boundaries B2 and B3) with increasing LRCs, we investigate how the network structures influence the spreading of the excitable waves on SWNs. The initial spreading of excitation through the system can be depicted by recording the time when each node is first excited, following the starting initiation at the center of the medium. The initial waves expand radially, after the central node is excited, via local and LRCs to destination nodes. These initiations continue to propagate until all of the nodes have been excited at least once. Figure 8(a) shows a typical con-

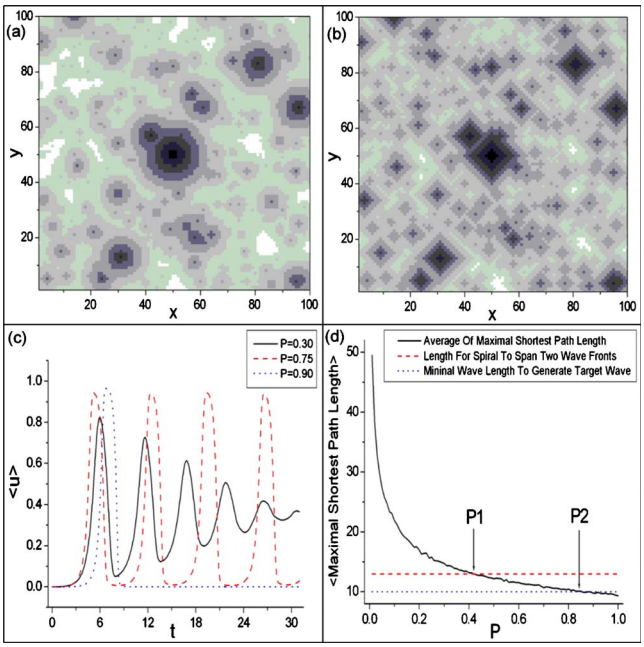

FIG. 8. (Color online) (a) The normalized excitation time needed from the central wave initiation to each node. (b) The normalized SPL from the central node to each node of the network of (a). The two distribution patterns of (a) and (b) are similar to each other, indicating wave propagation along the shortest pathway in excitable SWNs. (c) The evolutions of $\langle u(t)\rangle$ for three distinct network structures. Black solid, red dashed, and blue dotted curves show $\langle u(t)\rangle$ signals after the central wave initiation for $P=0.30$ (asymptotically nonsynchronizing oscillation), $P=0.75$ (asymptotically synchronizing oscillation), and $P=0.90$ (asymptotically rest state), respectively. (d) The average of the maximal SPL versus the LRC probability P. The red dashed line is the length for perfect spiral waves to span two wave arms. The blue dotted line is the minimal wavelength to generate target waves via LRC pacing. The crossing P values $\hat{P}_1 \approx 0.42$ and $\hat{P}_2 \approx 0.85$ are approximately equal to the discontinuous transitions around 0.45 (from nonsynchronizing oscillation to synchronizing oscillation) and 0.82 (from synchronizing oscillation to the rest state), respectively.

figuration for $P=0.10$, where each node is shaded according to the normalized excitation time after the central site of the medium is excited. Lots of target-wave-like patterns can be seen and from which we can find the wave spreading pathway from the central excitation through various local couplings and LRCs.

On the other hand, the network structure can be described by using the SPL between each node and the central node in the network. Figure 8(b) shows the network structure same as in Fig. 8(a), where each node is shaded according to its normalized distance from the central node along the shortest pathway. The striking similarity between Figs. 8(a) and 8(b) indicates that excitable waves propagate through the network via the shortest path between nodes. Therefore, the network structure of the excitable SWN is closely related to the spatiotemporal dynamics of the system. The LRC probability P is a crucial parameter determining the network structure. Figure 8(c) shows the evolutions of $\langle u(t)\rangle$ after the central node of the medium is excited for three different values of P. To our surprise, even for rather small P (when asymptotically nonsynchronizing oscillations are observed in Figs. 1–3) synchronizing oscillation can be clearly seen at early several periods [see the black solid curve in Fig. 8(c)]. For small P this synchronizing oscillation cannot persist and it is replaced with spiral waves in asymptotic motions due to the wave propagation through local couplings. The red dashed curve shows the persistent synchronizing oscillation at fairly large P ($P=0.75$), while for even larger P synchronizing oscillation can damp after early synchronizing oscillatory transient [see the blue dotted curve in Fig. 8(c)]. From all the three curves in Fig. 8(c), we realize that the synchronizing oscillations are always existent at the early evolutions after initiations. Due to the different network structures, these early synchronizing motions can be suppressed (with low P, $P<P_1$), persistently (with fairly large P, $P_1<P<P_2$) and damped (with too large P, $P>P_2$) for different P's. Then we are faced with a question of why the synchronizing oscillation can be suppressed or can damp for too low or too large LRC probabilities, respectively.

To answer the above question, we calculate SPLs for different sets of LRC probabilities P's and record the SPLs for each test and then find the maximal SPL from each of 50 samples for a given P. Figure 8(d) shows the average of the maximal SPL among 50 samples versus the LRC probability P. There are two characteristic horizontal lines shown in Fig. 8(d): the red dashed line is the length for perfect spiral waves to span two wave arms in the corresponding regular medium and the blue dotted line is the minimal wavelength to generate target waves via LRC pacings. With increasing of P the average of the maximal SPL decays exponentially and intersect with the red and blue lines, successively. When the maximal SPL is above this red dashed line, excitation waves can propagate in sufficiently large space and two spiral wave arms (one is a spiral tip and the other is a wave front) can be formed along this wave pathway, i.e., the phase of excitable wave on this pathway can be 4π. Because of the existence of the front wave arm which will collide with other waves, the spiral tips cannot be annihilated by other invading waves within a period and then the tips can survive during the evolution. Whenever spiral tips survive, spiral waves can self-sustain and can succeed to control the whole system. So the early synchronizing oscillations are suppressed. The intersection point locates at $\hat{P}_1 \approx 0.42$ which approximately agrees with the critical point for the nonsynchronizing-synchronizing oscillation transition at $P_1=0.45$. When the maximal SPL is below the blue dotted line, all nodes returning to the refractory state after excited by an excitation of the previous period cannot be excited again within so short period by the second initiation. So all the initiation excitations will be damping within a period, just like what happen in Fig. 8(c). The second intersection point locates at $\hat{P}_2 \approx 0.85$ which approximately coincides with the threshold at $P_2=0.82$, over which the system transits from synchronizing oscillation to the rest dead state.

VI. CONCLUSION

In conclusion we have investigated the spatiotemporal pattern formation in excitable media with small-world con-

nections. With increasing of the LRC probability P, five self-sustained oscillating patterns have been observed, such as the coexistence of pure spiral and pure target waves, patterns of mixtured spirals and target waves, pseudospiral turbulence, and synchronizing oscillations. The mechanisms underlying all these characteristically different oscillatory states are intuitively explained. In particular, we use the SPL analysis to explain the mechanism of the emergence of synchronizing oscillations and give predictions of the appearance and annihilation of the synchronizing oscillations by varying the LRC probability with good approximation. Since self-sustained oscillations in SWNs are a very important topic in wide practical fields such as neural networks, a systematical investigation of the phenomena and explanations of the mechanisms of various significant phenomena are expected to be useful both for theoretical understandings and practical applications.

ACKNOWLEDGMENTS

This work was supported by the National Natural Science Foundation of China under Grants No. 10675020 and No. 10975015 and by the National Basic Research Program of China (973 Program) under Grant No. 2007CB814800.

[1] E. Meron, Phys. Rep. **218**, 1 (1992).
[2] C. Cross and P. C. Hoheberg, Rev. Mod. Phys. **65**, 851 (1993).
[3] A. T. Winfree, *When Time Breaks Down* (Princeton University Press, Princeton, NJ, 1987).
[4] *Chemical Waves and Patterns*, edited by R. Kapral and K. Showalter (Kluwer, Dordrecht, 1995).
[5] A. N. Zaikin and A. M. Zhabotinsky, Nature (London) **225**, 535 (1970).
[6] X. Huang, W. C. Troy, Q. Yang, H. Ma, C. R. Laing, S. J. Schiff, and J. Y. Wu, J. Neurosci. **24**, 9897 (2004).
[7] M. A. Dahlem, F. M. Schneide, and E. Schóll, Chaos **18**, 026110 (2008).
[8] R. A. Gray, A. M. Pertsov, and J. Jalife, Nature (London) **392**, 75 (1998).
[9] A. Mikhailov, *Foundations of Synergetics* (Springer-Verlag, Berlin, 1994).
[10] D. J. Watts and S. H. Strogatz, Nature (London) **393**, 440 (1998).
[11] V. M. Eguiluz, D. R. Chialvo, G. A. Cecchi, M. Baliki, and A. V. Apkarian, Phys. Rev. Lett. **94**, 018102 (2005).
[12] F. Qi, Z. Hou, and H. Xin, Phys. Rev. Lett. **91**, 064102 (2003).
[13] A. Zumdieck, M. Timme, T. Geisel, and F. Wolf, Phys. Rev. Lett. **93**, 244103 (2004).
[14] L. F. Lago-Fernandez, R. Huerta, F. Corbacho, and J. A. Siguenza, Phys. Rev. Lett. **84**, 2758 (2000).
[15] D. He, G. Hu, M. Zhan, W. Ren, and Z. Gao, Phys. Rev. E **65**, 055204(R) (2002).
[16] S. Yonker and R. Wackerbauer, Phys. Rev. E **73**, 026218 (2006).
[17] A. Roxin, H. Riecke, and S. A. Solla, Phys. Rev. Lett. **92**, 198101 (2004).
[18] A. J. Steele, M. Tinsley, and K. Showalter, Chaos **16**, 015110 (2006).
[19] S. Sinha, J. Saramäki, and K. Kaski, Phys. Rev. E **76**, 015101(R) (2007).
[20] O. I. Kanakov, G. V. Osipov, C.-K. Chan, and J. Kurths, Chaos **17**, 015111 (2007).
[21] M. Perc, Chaos, Solitons Fractals **31**, 280 (2007).
[22] Q. L. X. Sun, M. Perc, and J. Kurths, Chaos **18**, 023102 (2008).
[23] A. Rothkegel and K. Lehnertz, Chaos **19**, 015109 (2009).
[24] D. Guo and C. Li, IEEE Trans. Neural Netw. **21**, 895 (2010).
[25] Y. Qian, X. Huang, G. Hu, and X. Liao, Phys. Rev. E **81**, 036101 (2010).
[26] M. Bär and M. Eiswirth, Phys. Rev. E **48**, R1635 (1993).